

Guided Multi-Fidelity Bayesian Optimization for Data-driven Controller Tuning with Digital Twins

Mahdi Nobar*, Jürg Keller†, Alessandro Forino‡, John Lygeros§, and Alisa Rupenyan¶

Abstract—We propose a *guided multi-fidelity Bayesian optimization* (GMFBO) framework for data-efficient controller tuning that integrates corrected digital twin (DT) simulations with real-world measurements. The method targets closed-loop systems with limited-fidelity simulations or inexpensive approximations. To address model mismatch, we build a multi-fidelity surrogate with a learned correction model that refines DT estimates from real data. An adaptive cost-aware acquisition function balances expected improvement, fidelity, and sampling cost. Our method ensures adaptability as new measurements arrive. The accuracy of DTs is re-estimated, dynamically adapting both cross-source correlations and the acquisition function. This ensures that accurate DTs are used more frequently, while inaccurate DTs are appropriately downweighted. Experiments on robotic drive hardware and supporting numerical studies demonstrate that our method enhances tuning efficiency compared to standard Bayesian optimization (BO) and multi-fidelity methods.

Index Terms—Multi-fidelity Bayesian optimization, Gaussian processes, Adaptive learning control, Smart Manufacturing

I. INTRODUCTION

In controller tuning, cost-effective simulation tools like Simulink, Gazebo, PyBullet, and LabVIEW have become essential, minimizing the need for expensive real-world experiments alongside digital twins [1]. Although digital twins often exhibit discrepancies when replicating real-world system behavior, they are nonetheless capable of capturing key operational dynamics and trends—making them valuable tools for informed optimization tasks [2]. Low-cost simulations, although less accurate, offer faster and cheaper evaluation cycles compared to high-fidelity experiments [3], [4]. For instance, they have been successfully employed in intelligent manufacturing to accelerate optimization processes [5], [6]. These simulations can enhance performance even at reduced fidelity [7], facilitating rapid prototyping and testing while decreasing reliance on costly physical experiments [8], [9].

To leverage simulations with varying fidelities, Multi-Fidelity Bayesian Optimization (MFBO) has been developed, incorporating multiple information sources with different fidelity and cost levels [10], [11]. MFBO balances the trade-

Maxon Motor AG and Swiss National Science Foundation supported this work through NCCR Automation, grant number 180545. (Corresponding author: Mahdi Nobar.)

* mnobar@ethz.ch Automatic Control Laboratory, ETH Zürich, Switzerland.

† juerg.keller@fhnw.ch Automation Institute, FHNW, Switzerland.

‡ alessandro.forino@maxongroup.com Robotic Drive Systems, Maxon Motor AG, Sachseln, Switzerland.

§ jlygeros@ethz.ch Automatic Control Laboratory, ETH Zürich, Switzerland.

¶ alisa.rupenyan@zhaw.ch ZHAW Zurich University for Applied Sciences, ZHAW Centre for AI, Switzerland.

off between high-fidelity accuracy and low-fidelity efficiency, enabling more effective optimization strategies [12]. For example, [13] demonstrates MFBO in gait design for a soft quadruped, using simulation data alongside minimal physical trials to refine its controller. Advanced MFBO methods also account for input-dependent fidelities, where the discrepancy between low- and high-fidelity models varies with the decision variables. For instance, in robotics, a simulator may align well with the real system at nominal joint speeds (decision-variable settings) but deviate significantly at high accelerations. Such methods enhance data efficiency and robustness [14], underscoring the potential of integrating additional data to improve the precision and reliability of controller tuning [15].

Recent works have explored online learning methods to improve control performance under changing system dynamics [16]. Optimization has advanced through correction models that align simulations with real-world data, enabling the creation of more accurate models [17]. These developments facilitate tuning frameworks where both controller and twin are updated during optimization, thereby enhancing data efficiency and robustness to changes in the real system [18], [19].

The primary objective of this work is to improve the integration of digital twin data with real-system measurements, increase the data efficiency of BO-based controller tuning, and enable adaptivity to dynamic changes in the real system during optimization. We assume that data from the real system is expensive to acquire, while DT simulations are cheaper but of limited and variable accuracy. An important question we address is: *How can DTs of varying accuracy help optimize system performance?* To this end, our contributions are:

- A GMFBO framework for data-efficient controller tuning that integrates real and simulated data.
- A correction mechanism that refines DT predictions and quantifies their accuracy to guide optimization.
- An adaptive surrogate model that adjusts cross-source correlations based on DT accuracy.
- A cost-aware acquisition function that balances fidelity, expected improvement, and sampling cost, mitigating reliance on inaccurate DTs.
- Experimental validation on a robotic drive system, including experiments with changing real-system friction, demonstrating substantial improvements in tuning efficiency over baseline methods.

II. CONTROLLER TUNING PROBLEM

The *target information source* (IS1) is a closed-loop feedback system comprising the plant, controller, and associated components. We make no assumptions about the parametric

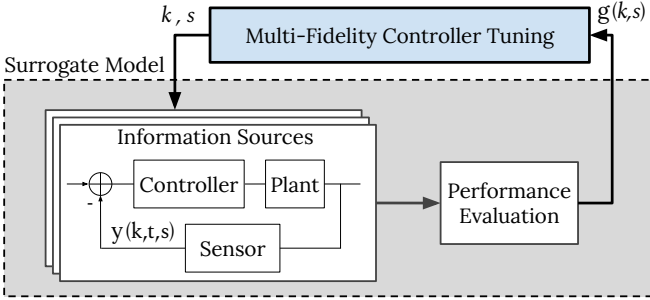


Fig. 1: Efficient controller parameters tuning based on multiple information sources

controller and plant structures. Measurements from IS1 are accurate up to measurement noise. An additional information source (IS2) serves as the system's *digital twin*. In many practical scenarios, the digital twin—constructed using physics-based modeling, empirical data, or a combination thereof—cannot be perfectly identified due to limited access to internal states, safety constraints, time limitations, or prohibitive data collection costs. Consequently, throughout the paper, we treat IS2 as less accurate than IS1. By accuracy (or fidelity), we mean the agreement between IS2's predicted objective and IS1's measured objective under identical controller parameters, formally defined in (12). Fig. 1 visualizes the problem setup.

Let $k \in \mathcal{K}$ be the *controller parameter vector* inside a known feasible set $\mathcal{K} \subseteq \mathbb{R}^{n_r}$. We choose the set \mathcal{K} so that the step response of the target system and its digital twin are bounded in a fixed period T . We define $s \in [0, 1]$ as a fidelity variable correlated with the accuracy of the information source. Here, $s = 1$ denotes IS1 (highest fidelity), while smaller values indicate lower fidelity. Let $s' < 1$ denote the fidelity level associated with IS2. The augmented input random variable is $z := [k, s]$ where $z \in \mathcal{K} \times \mathcal{S}$, with dimension $n_z := n_k + 1$. Let $\hat{g}(z) \in \mathbb{R}$ such that $\hat{g}(z) : \mathcal{K} \times \mathcal{S} \rightarrow \mathbb{R}$ denote the information source-dependent objective function. There is no assumption on the convexity of the objective function.

We evaluate an information source s at a given controller parameter k , measuring the feedback system *output* $y(k, t, s) \in \mathbb{R}$ at time $t \in \mathbb{R} \subseteq [0, T]$. We aim to simultaneously optimize $n_h > 1$ performance metrics denoted by $h_i(y(k, t, s)) \in \mathbb{R}$ for $i = 1, \dots, n_h$. These metrics quantify various aspects of system behavior, derived from measurable outputs relative to specified or desired references. We adopt a weighted sum approach to convert the multi-objective problem into a single-objective formulation [20], assigning relative importance to each performance metric [21]. So the overall performance cost function $\hat{f}(k)$ is

$$\hat{g}(k, s) := \mathbf{w}^\top \mathbf{h}(y(k, t, s)) = \sum_{i=1}^{n_h} w_i h_i(y(k, t, s)), \quad (1)$$

where $\mathbf{h}(k) := [h_1(k), \dots, h_{n_h}(k)]$ and $\mathbf{w} := [w_1, \dots, w_{n_h}]$. The weights vector \mathbf{w} adjusts the priority and scale of our metrics such that each metric properly contributes to the overall performance.

The data collection process is subject to measurement noise. Thus, a noisy observation g at input z is modeled as

$$g(z) = \hat{g}(z) + \eta, \quad (2)$$

where $\eta \sim \mathcal{N}(0, \sigma_\eta^2)$ denotes zero-mean Gaussian noise with variance σ_η^2 , estimated jointly with the kernel hyperparameters by maximizing the marginal log-likelihood [22]. This assumption is widely used because it effectively captures a broad range of independent random error sources, as per the central limit theorem [23]. We can imagine our information source including a performance assessment unit as a *black-box*, which provides the cost value $g(z)$ given the controller parameter vector k . Now our *data-driven controller tuning problem* is to obtain the optimum controller parameter vector k^* for IS1 by solving

$$k^* := \arg \min_{k \in \mathcal{K}} \hat{g}(k, s = 1). \quad (3)$$

Evaluating the objective function $\hat{g}(k, s = 1)$ is expensive, since it involves operating the real setup.

III. GUIDED MULTI-FIDELITY BAYESIAN OPTIMIZATION

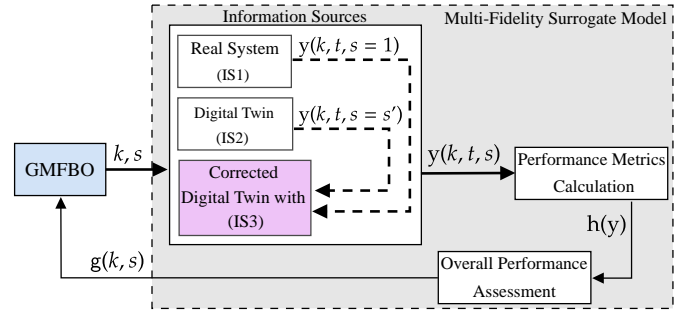


Fig. 2: Overall schematic of our proposed guided multi-fidelity Bayesian optimization for tuning controller parameters

Fig. 2 depicts our GMFBO framework. We first describe the surrogate objective model used in BO. Next, after defining the new information source and estimating DT accuracy, we present the adaptive surrogate kernel and acquisition function, followed by the GMFBO algorithm.

A. Multi-fidelity Surrogate Model

We define a *surrogate* Gaussian process to model the multi-fidelity objective $\hat{g}(z)$. We assume a GP prior over the function values $\mathbf{g}(\mathbf{z}) \sim \text{GP}(\mathbf{m}(\mathbf{z}), \mathbf{c}(\mathbf{z}))$, where $\mathbf{g}(\mathbf{z}) := [g(z_1), \dots, g(z_{N_0+n})]^\top$ represents the vector of function values at specific training points $\mathbf{z} := [z_1, \dots, z_{N_0+n}]$, prior means $\mathbf{m}(\mathbf{z}) := [m(z_1), \dots, m(z_{N_0+n})]^\top$, prior covariances $\mathbf{c}(z) := [c(z, z_1), \dots, c(z, z_{N_0+n})]^\top$, n is the number of observed points, \mathbf{m} and \mathbf{c} are the prior mean and covariance functions, respectively, $N_0 := N_{0_{s=1}} + N_{0_{s'}}$ is the total size of initial data set

$$\mathcal{D}_{\text{init}} := \{(z_i, g(z_i)) \mid i \in \{1, \dots, N_0\}\}, \quad (4)$$

where $N_{0_{s=1}}$ is the initial IS1 data size and $N_{0_{s'}}$ the initial IS2 data size. The likelihood function for n observations is then $p(\mathbf{g}|\mathbf{z}, \hat{\mathbf{g}}) = \mathcal{N}(\hat{\mathbf{g}}, \Sigma)$, where $\Sigma = \text{diag}(\sigma_{\eta_1}^2, \dots, \sigma_{\eta_n}^2)$ is a diagonal matrix of observational noise variances. We define *surrogate training dataset* $\mathcal{D} \in \mathbb{R}^{(n+N_0) \times (n_z+1)}$ with $n + N_0$ data points

$$\mathcal{D} := \{(z_i, g(z_i)) \mid i \in \{1, \dots, n + N_0\}\}. \quad (5)$$

The predictive distribution of $\hat{g}(z_*)$ at a test point z_* is $\hat{g}(z_*)|\mathcal{D} \sim \mathcal{N}(\mu_*, \sigma_*^2)$, where the predictive mean and variance are respectively $\mu_* := m(z_*) + \mathbf{c}(z_*)^T(\mathbf{C} + \boldsymbol{\Sigma})^{-1}(\mathbf{g}(\mathbf{z}) - \mathbf{m}(\mathbf{z}))$, and $\sigma_*^2 := c(z_*, z_*) - \mathbf{c}(z_*)^T(\mathbf{C} + \boldsymbol{\Sigma})^{-1}\mathbf{c}(z_*)$, with $\mathbf{c}(z_*)$ being the covariance vector between z_* and the training data, and $\mathbf{C} := [c(z_{\xi_1}, z_{\xi_2})] \Big|_{\xi_1, \xi_2=1}^{N_0+n} \in \mathbb{R}^{(N_0+n) \times (N_0+n)}$ [22].

B. Digital Twin Correction

Rather than modifying the objective function \hat{g} , the proposed approach focuses on improving the digital twin's state estimation through a learned correction. We propose a *correction model*, denoted by GP_c , to refine the simulation output acquired from IS2 given the controller gains k , resulting in a *corrected digital twin* (IS3). This model is a Gaussian process regression model [22] trained to predict the output signal $y(k, t, s = 1)$ from IS1 using the estimated state $y(k, t, s = s')$ from IS2 at time t . The correction model is trained on *correction dataset*, a dataset of paired observations defined by

$$\mathcal{D}_c := \{([t, y(k, t, s = s')], y(k, t, s = 1)) \mid t \in [0, T]\}, \quad (6)$$

where T is the period of data samples. The GP model assumes a homoscedastic Gaussian observation noise,

$$y(k, t, s = 1) = \hat{y}(k, t, s = 1) + \epsilon, \quad (7)$$

where $\epsilon \sim \mathcal{N}(0, \sigma_\epsilon^2)$ is the output measurement noise with variances σ_ϵ^2 which are jointly estimated with the kernel hyperparameters by maximizing the marginal log-likelihood [22]. Before training, both the inputs and targets are standardized to zero mean and unit variance, ensuring numerically stable hyperparameter learning [24].

We set the total number of BO iterations on IS1 and IS2 as N . Each time the optimizer samples IS1 at controller gains k , we add n_c new IS3 samples to \mathcal{D} (see Algorithm 1). For this, we draw $k' \sim \mathcal{N}(k, 0.05 \mathbb{K}) \in \mathcal{K}$, where \mathbb{K} is diagonal with entries equal to the feasible parameter ranges in \mathcal{K} . The factor 0.05 sets the per-parameter standard deviation to 5% of its range (elementwise, since \mathbb{K} is diagonal), thereby localizing IS3 evaluations near the latest IS1 point. If a draw falls outside \mathcal{K} , we project k' back onto \mathcal{K} . We found that using 2–10% yields similar behavior. The reference output signal is denoted as $y^*(t) \in \mathbb{R}$ for the feedback control system. Then, IS2 generates a sequence of estimated outputs $y(k', t, s')$ for $t = 0, \dots, T$, yielding corresponding inputs $[t, y(k', t, s')]$ for the correction model GP_c which then *predicts* the corrected estimation of the system output $\hat{y}(k', t, s = 1)$, denoted by

$$\hat{y}(k', t, s = 1) := \mu_c([t, y(k', t, s')]). \quad (8)$$

The standard deviation of this prediction is then denoted by $\sigma_c([t, y(k', t, s')])$. We define the prediction uncertainty as

$$\bar{\sigma}_c := \sqrt{\frac{1}{T} \sum_{t=0}^T \sigma_c^2([t, y(k', t, s')])}, \quad (9)$$

which measures the average predictive standard deviation of GP_c across the trajectory and reflects the reliability of the correction model. We impose the condition

$$\bar{\sigma}_c \ll \alpha := \sqrt{\frac{1}{T} \sum_{t=0}^T y^*(t)} \in \mathbb{R}, \quad (10)$$

with the threshold $\alpha \in \mathbb{R}$ serving as a normalized upper bound for acceptable uncertainty in IS3. If (10) holds, the model is deemed confident, and the data point is added as

$$\mathcal{D} \leftarrow \mathcal{D} \cup \{[k', s'], g_c(k', s')\}. \quad (11)$$

where $g_c(k', s')$ is the performance estimated using IS3. For each IS1 query, this procedure is repeated to generate n_c accepted IS3 samples that are added to \mathcal{D} . *Example:* For a unit step reference $y^*(t) = 1$ for $t \geq 0$, we obtain $\alpha = 1$. Here, α equals 100% of the normalized reference output, so $\bar{\sigma}_c \ll 1$ ensures the model's uncertainty remains small relative to maximum expected magnitude.

Each time $g_c(k', s')$ is estimated by IS3, the corresponding $y(k', t, s')$ samples from IS2 are already available, so computing $g_c(k', s')$ incurs no additional cost. We quantify the accuracy of IS2 relative to IS3 by

$$\hat{e}_{\text{IS2}} := \frac{1}{N_c} \sum_{i=1}^{N_c} \frac{|g_c(k'_i, s') - g(k'_i, s')|}{|g_c(k'_i, s')|}, \quad (12)$$

where N_c is the total number of IS3 samples in \mathcal{D} .

C. Adaptive Multi-Source Kernel Function

Building on the kernel formulation proposed for multi-fidelity GP models in [25], [26], we define the composite surrogate kernel as

$$c(z_1, z_2) := \gamma_0(s_1, s_2, \hat{e}_{\text{IS2}}) c_0(k_1, k_2) + \gamma_1(s_1, s_2) c_1(k_1, k_2), \quad (13)$$

with components

$$c_i(k_1, k_2) := \sigma_i^2 \mathcal{M}(\|k_1 - k_2\|, l_i), \quad i \in \{0, 1\}, \quad (14)$$

$$\gamma_0(s_1, s_2, \hat{e}_{\text{IS2}}) := \mathcal{M}(\|s_1 - s_2\|, l_{\gamma_0}(\hat{e}_{\text{IS2}})), \quad (15)$$

$$\gamma_1(s_1, s_2) := (1 - s_1)(1 - s_2)(1 + s_1 s_2)^p,$$

where $\mathcal{M}(r, l) := \left(1 + \frac{\sqrt{5}r}{l} + \frac{5r^2}{3l^2}\right) \exp\left(-\frac{\sqrt{5}r}{l}\right)$ is the Matérn-5/2 kernel, σ_i^2 are output variances, and p modulates correlation among sources with $s < 1$. The hyperparameters l_i , σ_i^2 , and p are learned via MAP estimation by maximizing the marginal log-likelihood with log-priors on l_i [22]. The mismatch metric \hat{e}_{IS2} from (12) adjusts γ_0 to reduce IS2-IS1 correlation when IS2 accuracy degrades. Here, $c_0(k_1, k_2)$ captures correlation between IS1 and IS2 as a function of controller-parameter distance, while γ_1 captures correlations among IS2 and IS3 data, and multiplication by $c_1(k_1, k_2)$ further incorporates controller-parameter similarity. Overall, the kernel jointly accounts for distances in controller space and fidelity-dependent correlations across all information sources.

To adapt the IS2-IS1 correlation to the estimated IS2 accuracy, we use the clamping operator $\mathcal{P}_{[a, b]}(x) := \min\{b, \max\{a, x\}\}$, which projects $x \in \mathbb{R}$ into $[a, b]$. Let $s' = \min(s_1, s_2)$. The cross-source lengthscale is defined as

$$l_{\gamma_0}(\hat{e}_{\text{IS2}}) := \mathcal{P}_{[l_{\gamma_0_{\min}}, l_{\gamma_0_{\max}}]} \left(\frac{s'}{\hat{e}_{\text{IS2}}} \right), \quad (16)$$

where \hat{e}_{IS2} is the normalized mismatch in (12). The clamp bounds $[l_{\gamma_0_{\min}}, l_{\gamma_0_{\max}}] := [0.1, 2]$ prevent under- or overfitting while keeping cross-source correlation responsive to \hat{e}_{IS2} .

Large \hat{e}_{IS2} (poor DT accuracy) pushes l_{γ_0} toward 0.2 (near-zero correlation), whereas small \hat{e}_{IS2} (high DT accuracy) drives it toward 2 (strong but not saturating correlation). We set $s' = 0.1$ as a heuristic to reflect the lower fidelity of the DT (IS2) relative to IS1. This choice also serves as a neutral pivot in (16): for $\hat{e}_{\text{IS2}} < s'$, the lengthscale increases (stronger cross-source coupling), while for $\hat{e}_{\text{IS2}} > s'$ it decreases (weaker coupling).

D. Adaptive Cost-aware Acquisition Function

We define the *fidelity-aware sampling cost* as

$$\mathcal{H}(s|\hat{e}_{\text{IS2}}) := \begin{cases} 1, & s = 1, \\ \mathcal{P}_{[\mathcal{H}_{\min}, \mathcal{H}_{\max}]}(\beta \cdot \hat{e}_{\text{IS2}}), & s \neq 1, \end{cases} \quad (17)$$

where $\beta \in \mathbb{R}$ is a constant scaling factor. Thus, IS1 evaluations always incur unit cost, while IS2 evaluations are scaled according to the estimated fidelity \hat{e}_{IS2} , with clamping to $[\mathcal{H}_{\min}, \mathcal{H}_{\max}] := [0.1, 1]$ ensuring numerical stability. We then define a *cost-aware Expected Improvement acquisition function* (caEI) as

$$\text{caEI}_n(z|\hat{e}_{\text{IS2}}) := \frac{a_{\text{EI},n}(z)}{\mathcal{H}(s|\hat{e}_{\text{IS2}})}, \quad (18)$$

where $a_{\text{EI},n}(z)$ is the expected improvement acquisition function with a closed-form formulation [27], computed independently for each information source. For fidelity s at iteration n , we write

$$a_{\text{EI},n}(z) := \sigma_n(z)(v_n(z)\Phi(v_n(z)) + \varphi(v_n(z))), \quad (19)$$

with $v_n(z) := (\mu_n(z) - g(s)^+)^{\sigma_n(z)^{-1}}$, where $\mu_n(z)$ and $\sigma_n(z)$ are the GP posterior mean and standard deviation, $g(s)^+$ is the best observed objective in fidelity s , $\Phi(\cdot)$ is the standard normal cdf, and $\varphi(\cdot)$ is the pdf.

For mechatronic systems with first-principles models, we expect $\beta = 4$ to be a reasonable starting point, so that high DT fidelity (small \hat{e}_{IS2}) yields values near 0.1—lowering the denominator of (18) and encouraging DT sampling—while low DT fidelity pushes the cost toward 1, discouraging reliance on inaccurate simulations. For a given \hat{e}_{IS2} , increasing β effectively decreases the sampling frequency from IS2; for instance, $\beta = 10$ results in less IS2 queries. Clamping avoids degenerate cases: the lower bound prevents division by a minimal denominator, and the upper bound ensures DT queries are never more expensive than real-system ones. This formulation enables the optimizer to adaptively switch between IS1 and IS2 based on the current accuracy of the DT, thereby promoting data efficiency while maintaining robustness.

E. Guided Multi-Fidelity BO Algorithm

Our GMFBO framework leverages real data not to build a globally accurate digital twin (DT), but to make it *objective-oriented*: the DT is selectively corrected in regions of the parameter space that are relevant for reaching the optimization objective. This distinguishes our approach from classical active learning, which focuses on improving model accuracy, aiming to enhance predictive fidelity everywhere.

Algorithm 1 summarizes the procedure. Real-system measurements are used to estimate the mismatch (12), which

in turn (i) adapts l_{γ_0} in (16) and \mathcal{H} in (17) to adjust the influence of simulated data, and (ii) updates the kernel in (13) to capture evolving fidelity-dependent correlations between real and simulated observations. At the acquisition level, the correction model modifies the sampling cost \mathcal{H} in (17), enabling the optimizer to balance exploration of the DT with the cost and reliability of real experiments.

In contrast to standard MFBO, which passively exploits correlations across fixed fidelities, GMFBO actively reshapes these correlations based on online mismatch estimates and focuses DT refinement only where it matters for optimization. This mechanism provides a direct pathway by which the DT and correction model *guide* the optimizer, as demonstrated in the following sections.

Algorithm 1 Guided Multi-Fidelity Bayesian Optimization

```

1: Initialize  $\mathcal{K}$ ,  $N$ ,  $N_{0_{s=1}}$ ,  $N_{0_s}$ ,  $n_c$ ,  $\mathcal{D}_c$ ,  $\text{GP}_c$ ,  $\mathcal{D} \leftarrow \mathcal{D}_{\text{init}}$ ,  

    $\hat{e}_{\text{IS2}}$ ,  $s'$ ,  $\alpha$ ,  $\beta$ 
2: for BO iteration  $n = 1, \dots, N$  do
3:   Train surrogate GP model given  $\mathcal{D}$ 
4:   Select candidate  $(k, s) \leftarrow \arg \max_{z=[k,s]} \text{caEI}_n(z|\hat{e}_{\text{IS2}})$ 
5:   if  $s = 1$  then
6:     Evaluate real system:  $(t, y(k, t, s), g(k, s)) \leftarrow \text{IS1}(k)$ 
7:     Update  $\mathcal{D} \leftarrow \mathcal{D} \cup \{[k, 1], g(k, s)\}$ 
8:     Evaluate DT:  $y(k, t, s') \leftarrow \text{IS2}(k)$ 
9:     Update  $\mathcal{D}_c \leftarrow \{([t, y(k, t, s')], y(k, t, 1)) \mid t \in [0, T]\}$ 
10:    Update correction model  $\text{GP}_c$ 
11:   while  $n_c$  new data from IS3 is not added to  $\mathcal{D}$  do
12:     Draw  $k' \in \mathcal{K}$ 
13:     Evaluate corrected DT:  $g_c(k', s') \leftarrow \text{IS3}(k)$ 
14:     if (10) is satisfied then
15:       Update  $\mathcal{D} \leftarrow \mathcal{D} \cup \{[k', s'], g_c(k', s')\}$ 
16:     end if
17:   end while
18:   Update simulation fidelity estimation:  $\hat{e}_{\text{IS2}}$ 
19:   Update  $l_{\gamma_0}$  and  $\mathcal{H}$  based on new  $\hat{e}_{\text{IS2}}$ 
20:   else if  $s = s'$  then
21:     Evaluate DT:  $g(k, s') \leftarrow \text{IS2}(k)$ 
22:     Update  $\mathcal{D} \leftarrow \mathcal{D} \cup \{[k, s'], g(k, s')\}$ 
23:   end if
24: end for
25: return  $k^* \leftarrow \arg \min_k g(k, s = 1), \forall (k, 1) \in \mathcal{D}$ 

```

IV. SYSTEM MODELLING

We employ the high-efficiency joint (HEJ) 90 drive system from maxon to iteratively tune the parameters of its joint position-velocity-torque (JPVT) controller. The system comprises a high-torque permanent magnet synchronous motor, a planetary gearbox, dual encoders, and power electronics, with an EPOS4 controller that features a hierarchical structure consisting of a low-level current loop and higher-level position, velocity, and torque loops. The JPVT controller uses a proportional-derivative position strategy with tunable parameters $k = (K_p, K_d)$, constrained by

$$\mathcal{K} = \{(K_p, K_d) \mid K_p \in [K_{p_{\min}}, K_{p_{\max}}], K_d \in [K_{d_{\min}}, K_{d_{\max}}]\}, \quad (20)$$

with $(K_{p_{\min}}, K_{p_{\max}}, K_{d_{\min}}, K_{d_{\max}}) = (30, 200, 2, 10)$ for numerical analysis and $(70, 120, 2, 5)$ for real experiments. Safety within \mathcal{K} can be enforced during optimization by incorporating barrier functions into g [28] or adopting safe exploration strategies [29].

Fig. 3a shows the information-source block diagram. Our objective is a weighted sum of four performance metrics from the position step response. A *unit* step reference $y^*(t) = 0$ for $t < t_0 = 0.1$ [s] and $y^*(t) = 1$ [rad] (652 encoder counts) for $0 \leq t - t_0 \leq T = 1$ [s] is applied to the motor output, yielding $\alpha = 1$ from (10). We define $h(k) = [O_s, T_{\text{tr}}, T_r, T_s]$, where O_s , T_{tr} , T_r , and T_s denote overshoot, transient, rise, and settling time, respectively. The objective function g for augmented input z is

$$g(z) = w_1 \cdot O_s + w_2 \cdot T_{\text{tr}} + w_3 \cdot T_r + w_4 \cdot T_s, \quad (21)$$

with weights $w_i, i = 1, \dots, 4$. Since \hat{e}_{IS2} in (12) is based on these metrics, the mismatch mainly reflects transient step-response errors, while effects outside this window or uncaptured by the metrics (e.g., backlash) may remain unobserved. To construct $\mathcal{D}_{\text{init}}$, we randomly sample (K_p, K_d) pairs from \mathcal{K} and record the resulting $h(k)$. The GP_c model is retrained whenever \mathcal{D}_c is updated. Fig. 3b illustrates IS3, where the learned model corrects DT outputs.

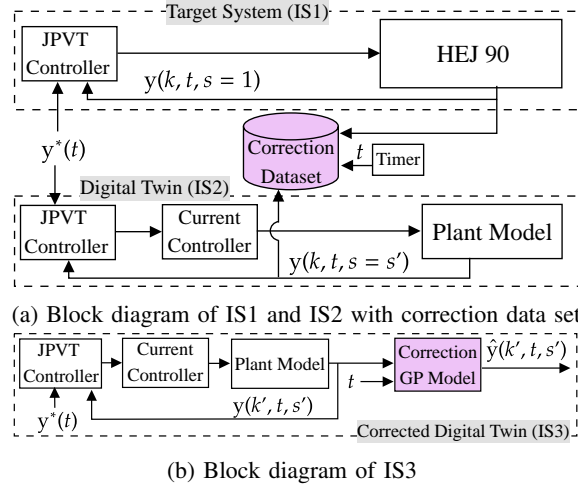


Fig. 3: Block diagrams of information sources

We employ a digital twin of the drive system (IS2), based on a nonlinear inverse flux linkage motor model [30] refined to account for friction, ripple harmonics, and a simple gearbox backlash model [31]. Table I summarizes the chosen values for the design parameters of our method.

TABLE I: Design Parameters of the GMFBO Method

Parameter	Expected Range	Chosen Value	Reference
$N_{0_{s=1}}$	≥ 1	2	Subsection V-A
$N_{0_{s'}}$	≥ 1	4	Subsection V-A
N	≥ 1	20	Algorithm 1
n_c	≥ 1	4	Algorithm 1
s'	$\in [0, 1]$	0.1	Section IV
α	$\in [0, 1]$	1	(10)
β	$\in [0, 10]$	4	(17)

V. NUMERICAL ANALYSIS

For the numerical analysis, IS1 is the original high-fidelity DT model from maxon with a lookup table mapping voltage to

current in the non-linear motor model. IS2 is identical, except that Gaussian noise with zero mean and standard deviation equal to 50% of the respective data range is added to the lookup table, reducing its accuracy.

Unless stated otherwise, we set $N_{0_{s=1}} = 2$, $N_{0_{s'}}$ = 10, and $N = 20$ BO iterations. The observation noise variance σ_η^2 is shared across information sources and estimated via GP marginal log-likelihood [32]. We use $n_c = 4$ corrected IS3 estimates and optimize the cost-aware EI in (18) with L-BFGS [33] to select the next candidate (k_{n+1}, s_{n+1}) . Objective weights and normalization are computed from 10 Latin Hypercube samples (LHS) [34], yielding $[w_1, w_2, w_3, w_4] = [0.02, 0.20, 0.70, 0.20]$, with means and standard deviations used for normalization of objectivess . Each tuning run is repeated $N_{\text{exper}} = 50$ times with $\mathcal{D}_{\text{init}}$ from random LHS samples. Let n^* be the average IS1 iterations to reach the optimum.

Fig. 4a shows the ground-truth objective over \mathcal{K} , where optimal regions occur at larger gains. Fig. 4b shows IS2 estimates with 20% relative error in $> 60\%$ of \mathcal{K} , but $> 50\%$ error in over 10% of the domain. Errors are largest away from the optimum, enabling the correction GP to refine DT accuracy in the optimal region and more effectively guide the optimizer.

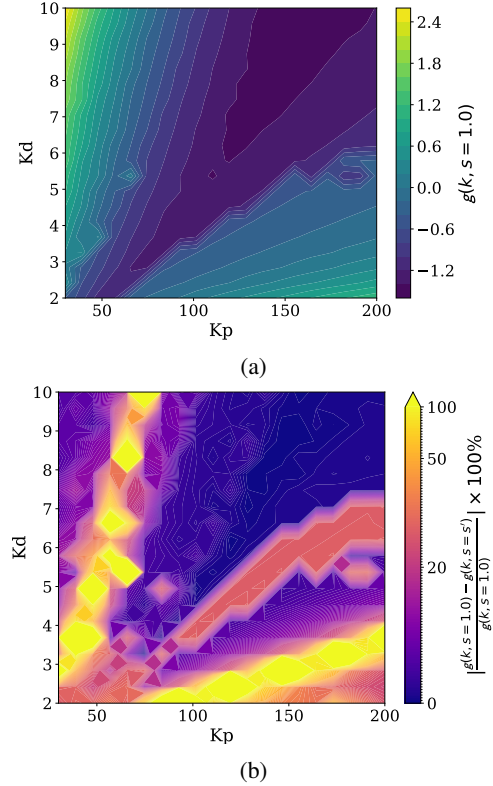


Fig. 4: (a) True objective function given IS1 and (b) relative absolute error (in %) of the estimated objective by IS2

A. Initial Dataset Ablation Study

Table II reports the required IS1 iterations (n^*) for different initial datasets. GMFBO performs best with a balanced amount of IS2 data: excess data degrades the surrogate due to IS2 inaccuracies, while insufficient data reduces efficiency. The benefit is most pronounced when IS1 samples are scarce.

TABLE II: Required n^* given different initial dataset sizes

		n^*		
$N_{0_{s=1}}$	$N_{0_{s'}}$	EI-BO	MFBO	GMFBO
1	10	15	> 21	9
2	10	22	> 22	6
3	10	17	> 23	10
4	10	17	> 24	11
5	10	15	> 25	11
10	10	20	> 30	15
2	5	22	> 22	13
2	20	20	> 22	10
2	30	22	> 22	10

B. Comparison with Baseline Methods

We compare GMFBO against baseline BO with Expected Improvement (EI) and three MFBO variants: baseline MFBO with trace-aware Knowledge Gradient (taKG) [35], baseline MFBO with our caEI, and a modified MFBO with caEI using the fidelity-aware kernel in (13) without IS3. The taKG acquisition weighs expected information gain against sampling cost, which relies strongly on the surrogate GP. GMFBO explicitly corrects DT bias and guides optimization toward the objective. In contrast, taKG resembles an active learning strategy that improves surrogate accuracy in informative regions without adapting to biased or shifting fidelities.

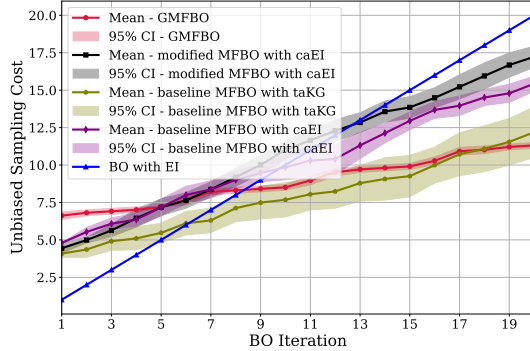


Fig. 5: Unbiased sampling cost over BO iterations, averaged over 50 Monte Carlo experiments. Shaded regions indicate 95% confidence intervals.

To compare sampling costs across IS selections, we define the *unbiased sampling cost* of an experiment with n data points as $\sum_{i=1}^{i=n} \mathcal{H}(s_i, \hat{e}_{IS2}) - b(\hat{e}_{IS2}) = \sum_{i=1}^{i=n} s_i$, which quantifies the number of samples acquired from each information source. Figure 5 shows the mean and confidence intervals (CI) of these costs for different methods. GMFBO has a higher initial sampling cost since $N_{0_{s=1}} \cdot n_c = 2 \cdot 4 = 12$ IS3 samples are required. Since IS3 is inexpensive and guides the optimizer to reduce IS1 queries, GMFBO attains a lower cumulative unbiased cost than BO and other MFBO methods, whose higher variance results from oversampling inaccurate DT data, inflating the sampling cost.

Fig. 6 shows that baseline MFBO with taKG (olive) fails to exploit IS2 and exhibits higher variance than MFBO with caEI (purple) due to poor acquisition. Large IS2 errors cause taKG to oversample inaccurate IS2 data, polluting the surrogate without adjusting fidelity influence. Since taKG estimates the optimum from the posterior GP, its failure arises from

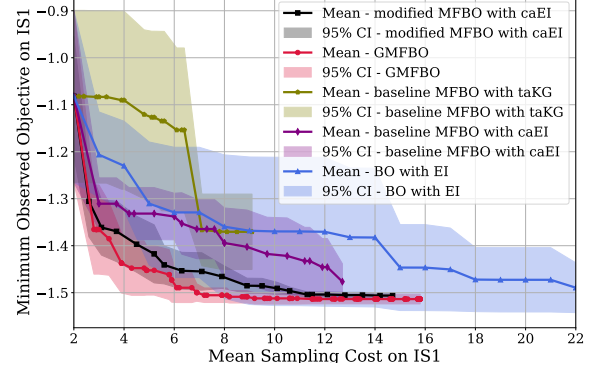


Fig. 6: Minimum observed IS1 objective vs. mean IS1 sampling cost over 50 Monte Carlo experiments. Shaded regions denote 95% confidence intervals

IS2's relative absolute error (Fig. 4b), which exceeds 20% on average. Using caEI improves the baseline MFBO to a level comparable to that of BO using EI, although without a clear reduction in CI. The modified MFBO (black) further benefits from the customized kernel, which shrinks variance by adjusting the influence of DT data in the surrogate and preventing optimizer pollution from low-accuracy DR data, leading to improved convergence. Our GMFBO, which combines caEI, a customized kernel, and IS3 correction, achieves higher data efficiency by requiring fewer IS1 measurements with reduced and faster-decreasing variability across iterations. BO and modified MFBO with caEI need 22 and 11 IS1 experiments on average (including initialization) to reach a given threshold, whereas GMFBO requires only 6, i.e., 72% and 45% fewer, respectively. In the best run, GMFBO converges in 2 experiments, compared to 8 and 6 for BO and modified MFBO, yielding 75% and 66% improvements. Even in the worst case, GMFBO converges within 8 experiments, while BO may not converge after 22, and modified MFBO requires 11, i.e., improvements of at least 64% and 27%. These results show that GMFBO outperforms BO and both baseline and modified MFBO methods.

C. Adaptation to System Variation

We study a non-stationary system where the motor friction coefficient in IS1 doubles after the fourth iteration of IS1, while IS2 remains unchanged, thereby reducing its fidelity.

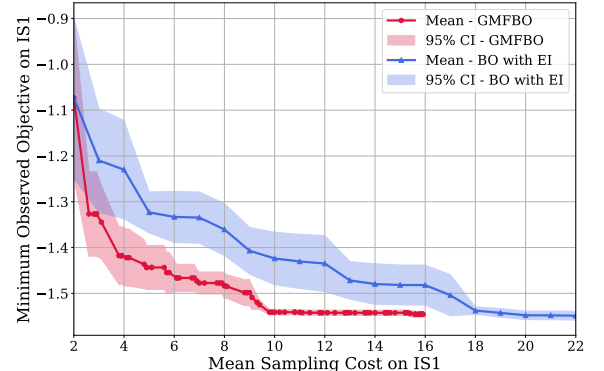


Fig. 7: Minimum observed IS1 objective vs. mean IS1 cost over 50 Monte Carlo experiments with varying friction in IS1. Shaded regions denote 95% confidence intervals

As shown in Fig. 7, GMFBO adapts to the IS1 change and finds the new optimum in 10 IS1 experiments, compared

to over 18 for BO with EI (44% improvement). The change increases IS2 error, which lowers cross-source correlation and raises IS2 sampling cost, while online IS3 corrections improve the surrogate. This allows GMFBO to continue exploiting DT data despite shifting system dynamics.

VI. HARDWARE EXPERIMENTAL RESULTS

We validate data efficiency and generalization on the Maxon HEJ 90 drive system (Fig. 8), with IS1 as the real hardware and IS2 as the DT (corresponding to IS1 in the previous section V). The integrated EPOS4 controller employs a hierarchical structure comprising current, position, velocity, and torque loops, all of which are accessed via EtherCAT. A custom MasterMACS–ApossIDE integration enables real-time acquisition of encoder positions and control inputs at 1 kHz [36].

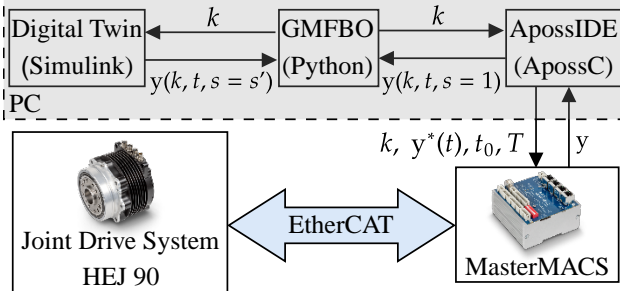


Fig. 8: Real system hardware setup used to evaluate GMFBO

Since the objective metrics (overshoot, rise, settling, and transient times) differ in scale and estimation accuracy, we normalize them and assign weights that reflect both application relevance and IS2 reliability. Weights can be adapted to task priorities or evolving DT accuracy; in our case, $w_1 = 0.01$, $w_2 = 0.09$, $w_3 = 0.82$, $w_4 = 0.09$.

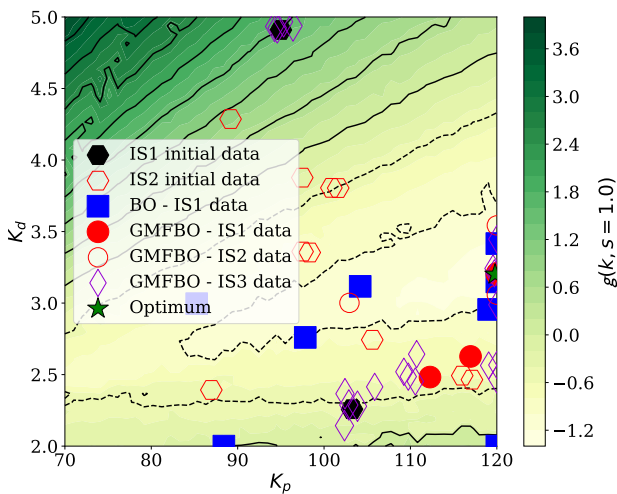


Fig. 9: Sampled data points of GMFBO and baseline BO with EI in a single experiment. Iterations are shown until the minimum objective approaches the global optimum (star). Contours depict the true objective.

Fig. 9 shows sampled data points per method in a single experiment until the optimum is found. Baseline BO relies heavily on costly IS1 measurements, whereas GMFBO shifts part of the exploration and exploitation to cheaper IS2 and IS3, reducing IS1 usage.

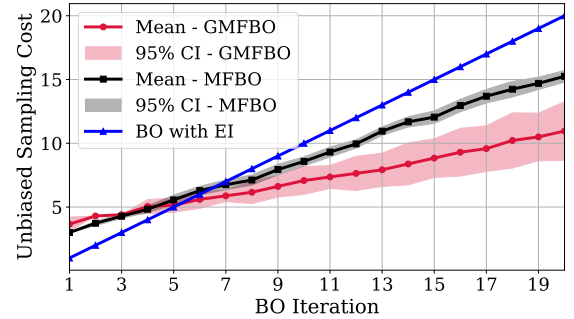


Fig. 10: Unbiased sampling cost over BO iterations from 20 Monte Carlo experiments. Shaded regions denote 95% confidence intervals.

We conduct a Monte Carlo analysis with $N_{\text{exper}} = 20$ experiments. Fig. 10 shows that our GMFBO method incurs lower total sampling cost than both BO and MFBO over $N = 20$ BO iterations. We also observe variability in the unbiased sampling cost for GMFBO and MFBO, stemming from the dynamic selection between two information sources guided by our acquisition function. Additionally, the confidence interval for GMFBO’s sampling cost is wider than that of MFBO, reflecting greater cost variability due to reliance of IS3 to the real system measurements.

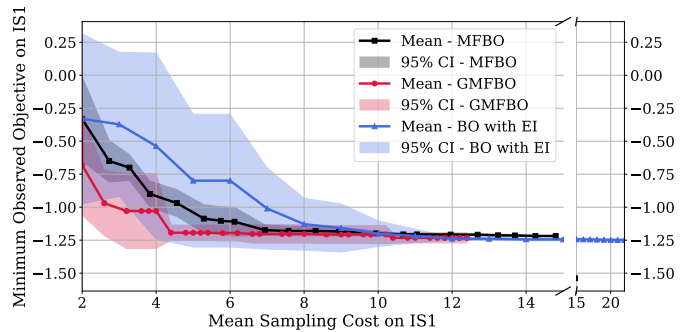


Fig. 11: Minimum observed IS1 objective vs. mean IS1 cost on the real system from 20 Monte Carlo experiments. Shaded denotes 95% confidence interval.

Fig. 11 shows that GMFBO requires fewer real-system experiments on average, with a smaller and faster-shrinking confidence interval than other methods. BO and MFBO need 9 and 7 experiments, respectively, while GMFBO achieves the same performance in only 5, yielding 44% and 28% improvements. Among the experiments, the best GMFBO converges in 2 experiments (vs. 6 for BO and 4 for MFBO, 67% and 50% improvements), and the worst in 6 (vs. 13 and 8, 54% and 25% improvements).

VII. CONCLUSION

This paper introduces a guided multi-fidelity Bayesian optimization (GMFBO) framework for data-efficient controller tuning, which systematically incorporates simulation fidelity into the surrogate model. Our main contributions are: (i) a customized multi-source kernel that adaptively scales cross-fidelity correlations based on estimated digital-twin accuracy, preventing low-fidelity data from degrading the surrogate; (ii) an adaptive cost-aware acquisition function that balances

sampling cost, fidelity, and expected improvement for efficient query selection; and (iii) integration of real-data corrections to maintain robustness under model mismatch and adapt to varying simulation fidelities.

Extensive numerical studies have shown that GMFBO consistently outperforms existing multi-fidelity methods in terms of convergence speed and sample efficiency. On robotic drive hardware, GMFBO achieved over 28% improvement in optimization efficiency compared to baselines.

These results demonstrate the potential of GMFBO to accelerate learning in systems with costly experiments and imperfect models. Future work will extend the framework to settings where fidelity varies with the controller gains (input-dependent) or the system's operating conditions (state-dependent, e.g., velocity or load). We also plan to investigate closed-loop, data-efficient digital twin identification and robustness under non-convex and discontinuous objectives.

REFERENCES

- [1] C. König, R. Krishnadas, E. C. Balta, and A. Rupenyan, “Adaptive bayesian optimization for high-precision motion systems,” *IEEE Transactions on Automation Science and Engineering*, pp. 1–1, 2025.
- [2] B. Soykan, G. Blanc, and G. Rabadi, “A proof-of-concept digital twin for real-time simulation: Leveraging a model-based systems engineering approach,” *IEEE Access*, vol. 13, pp. 58 899–58 912, 2025.
- [3] B. Park, A. Chen, and S. Mishra, “Real-time melt pool homogenization through geometry-informed control in laser powder bed fusion using reinforcement learning,” *IEEE Transactions on Automation Science and Engineering*, vol. 22, pp. 2986–2997, 2025.
- [4] S. He, A. von Rohr, D. Baumann, J. Xiang, and S. Trimpe, “Simulation-aided policy tuning for black-box robot learning,” *IEEE Transactions on Robotics*, vol. 41, pp. 2533–2548, 2025.
- [5] W. Meng, H. Ju, T. Ai, R. Gomez, E. Nichols, and G. Li, “Transferring meta-policy from simulation to reality via progressive neural network,” *IEEE Robotics and Automation Letters*, vol. 9, no. 4, pp. 3696–3703, 2024.
- [6] F. Garbuglia, D. Deschrijver, and T. Dhaene, “On the role of bayesian learning for electronic design automation: A survey,” *IEEE Electromagnetic Compatibility Magazine*, vol. 12, no. 4, pp. 77–84, 2023.
- [7] M. Nobar, J. Keller, A. Rupenyan, M. Khosravi, and J. Lygeros, “Guided bayesian optimization: Data-efficient controller tuning with digital twin,” *IEEE Transactions on Automation Science and Engineering*, vol. 22, pp. 11 304–11 317, 2025.
- [8] M. Wu, A. Rupenyan, and B. Corves, “Autogeneration and optimization of pick-and-place trajectories in robotic systems: A data-driven approach,” *Robotics and Computer-Integrated Manufacturing*, vol. 97, p. 103080, 2026. [Online]. Available: <https://www.sciencedirect.com/science/article/pii/S0736584525001346>
- [9] J. Gao, M. Y. Michelis, A. Spielberg, and R. K. Katzschnann, “Sim-to-real of soft robots with learned residual physics,” *IEEE Robotics and Automation Letters*, vol. 9, no. 10, pp. 8523–8530, 2024.
- [10] M. C. Kennedy and A. O’Hagan, “Predicting the output from a complex computer code when fast approximations are available,” *Biometrika*, vol. 87, no. 1, pp. 1–13, 2000.
- [11] A. I. Forrester, A. Sóbester, and A. J. Keane, “Multi-fidelity optimization via surrogate modelling,” *Proceedings of the royal society a: mathematical, physical and engineering sciences*, vol. 463, no. 2088, pp. 3251–3269, 2007.
- [12] Q. Lin, J. Hu, Q. Zhou, L. Shu, and A. Zhang, “A multi-fidelity bayesian optimization approach for constrained multi-objective optimization problems,” *Journal of Mechanical Design*, vol. 146, no. 7, p. 071702, 01 2024. [Online]. Available: <https://doi.org/10.1115/1.4064244>
- [13] K. Tan, X. Niu, Q. Ji, L. Feng, and M. Törngren, “Optimal gait design for a soft quadruped robot via multi-fidelity bayesian optimization,” *Applied Soft Computing*, vol. 169, p. 112568, 2025. [Online]. Available: <https://www.sciencedirect.com/science/article/pii/S1568494624013425>
- [14] M. Fan, B.-J. Yoon, E. Dougherty, F. Alexander, N. Urban, R. Arróyave, and X. Qian, “Multi-fidelity bayesian optimization with multiple information sources of input-dependent fidelity,” in *The 40th Conference on Uncertainty in Artificial Intelligence*, 2024.
- [15] Y. Zhang, S. Park, and O. Simeone, “Multi-fidelity bayesian optimization with across-task transferable max-value entropy search,” *IEEE Transactions on Signal Processing*, vol. 73, pp. 418–432, 2025.
- [16] Y. Meng, Z. Bing, X. Yao, K. Chen, K. Huang, Y. Gao, F. Sun, and A. Knoll, “Preserving and combining knowledge in robotic lifelong reinforcement learning,” *Nature Machine Intelligence*, pp. 1–14, 2025.
- [17] Z. Shen, F. Arraño-Vargas, and G. Konstantinou, “Development of adaptive model-based digital twins for evolving power systems,” *Computers and Electrical Engineering*, vol. 125, p. 110418, 2025.
- [18] X. Tong, Q. Liu, Y. Zhou, and P. Sun, “A digital twin-driven cutting force adaptive control approach for milling process,” *Journal of Intelligent Manufacturing*, vol. 36, no. 1, pp. 551–568, 2025.
- [19] J. P. Allamaa, P. Patrinos, H. Van der Auweraer, and T. D. Son, “Learning-based nmpc adaptation for autonomous driving using parallelized digital twin,” *IEEE Transactions on Control Systems Technology*, 2024.
- [20] J. L. J. Pereira, G. A. Oliver, M. B. Francisco, S. S. Cunha Jr, and G. F. Gomes, “A review of multi-objective optimization: methods and algorithms in mechanical engineering problems,” *Archives of Computational Methods in Engineering*, vol. 29, no. 4, pp. 2285–2308, 2022.
- [21] J.-h. Ryu, S. Kim, and H. Wan, “Pareto front approximation with adaptive weighted sum method in multiobjective simulation optimization,” in *Proceedings of the 2009 Winter Simulation Conference (WSC)*, 2009, pp. 623–633.
- [22] C. K. Williams and C. E. Rasmussen, *Gaussian processes for machine learning*. MIT press Cambridge, MA, 2006, vol. 2, no. 3.
- [23] S. Thrun, W. Burgard, and D. Fox, *Probabilistic Robotics (Intelligent Robotics and Autonomous Agents)*. The MIT Press, 2005.
- [24] The MathWorks, Inc., *Statistics and Machine Learning Toolbox: fitrgp function*, 2025, version R2025a. [Online]. Available: <https://ch.mathworks.com/help/stats/fitrgp.html>
- [25] M. Poloczek, J. Wang, and P. Frazier, “Multi-information source optimization,” *Advances in Neural Information Processing Systems*, vol. 30, 2017, see p. 3, Subsection 3.1, Supplementary Material, p. 15, Subsection B.1.
- [26] H. Rakotoarison, S. Adriaensen, N. Mallik, S. Garibov, E. Bergman, and F. Hutter, “In-context freeze-thaw bayesian optimization for hyperparameter optimization,” in *Proceedings of the 41st International Conference on Machine Learning*, ser. ICML’24. JMLR.org, 2024.
- [27] H. Zhou, X. Ma, and M. B. Blaschko, “A corrected expected improvement acquisition function under noisy observations,” in *Proceedings of the 15th Asian Conference on Machine Learning*, ser. Proceedings of Machine Learning Research, B. Yanıkoglu and W. Buntine, Eds., vol. 222. PMLR, 11–14 Nov 2024, pp. 1747–1762. [Online]. Available: <https://proceedings.mlr.press/v222/zhou24a.html>
- [28] M. Khosravi, C. König, M. Maier, R. S. Smith, J. Lygeros, and A. Rupenyan, “Safety-aware cascade controller tuning using constrained bayesian optimization,” *IEEE Transactions on Industrial Electronics*, vol. 70, no. 2, pp. 2128–2138, 2023.
- [29] C. König, M. Ozols, A. Makarova, E. C. Balta, A. Krause, and A. Rupenyan, “Safe risk-averse bayesian optimization for controller tuning,” *IEEE Robotics and Automation Letters*, vol. 8, no. 12, pp. 8208–8215, 2023.
- [30] K. Drobnič, L. Gašparin, and R. Fišer, “Fast and accurate model of interior permanent-magnet machine for dynamic characterization,” *Energies*, vol. 12, no. 5, 2019.
- [31] MathWorks, *Gear with Backlash*, The MathWorks, Inc., 2024, accessed: 2025-07-15. [Online]. Available: <https://ch.mathworks.com/help/sdl/ug/gear-with-backlash.html>
- [32] M. Balandat, B. Karrer, D. Jiang, S. Daulton, B. Letham, A. G. Wilson, and E. Bakshy, “Botorch: A framework for efficient monte-carlo bayesian optimization,” *Advances in neural information processing systems*, vol. 33, pp. 21 524–21 538, 2020.
- [33] D. C. Liu and J. Nocedal, “On the limited memory bfgs method for large scale optimization,” *Mathematical Programming*, vol. 45, no. 1, pp. 503–528, Aug 1989. [Online]. Available: <https://doi.org/10.1007/BF01589116>
- [34] R. L. Iman, J. C. Helton, and J. E. Campbell, “An approach to sensitivity analysis of computer models: Part i—introduction, input variable selection and preliminary variable assessment,” *Journal of quality technology*, vol. 13, no. 3, pp. 174–183, 1981.
- [35] J. Wu, S. Toscano-Palmerin, P. I. Frazier, and A. G. Wilson, “Practical multi-fidelity bayesian optimization for hyperparameter tuning,” in *Uncertainty in Artificial Intelligence*. PMLR, 2020, pp. 788–798.
- [36] maxon, “Robotics solutions — high-torque density motors and controllers,” <https://www.maxongroup.com/en/market-solutions/mobility-solutions/robotics>, accessed: 2025-07-15.